Quarterly Progress Report

This report covers the period of June 15, 2016 to September 14, 2016

Submitted to

The Office of Naval Research

Project Title: Noise of High-Performance Aircraft at Afterburner

Principal Investigator

Dr. Christopher Tam

Department of Mathematics

Florida State University

Email: tam@math.fsu.edu

Grant Monitor

Dr. John Spyropoulous

Email: John.Spyropoulous@jsf.mil

There are two elements in this project. They are,

1. Analysis of the noise of high-performance military aircraft.
2. Investigation of the importance of indirect combustion noise as a dominant component of military aircraft noise at afterburner.

This quarterly progress report concentrates on the second element of the project.

I. Introduction

When extra fuel is burnt at afterburner operating condition, the combustion process is highly unsteady. This creates large temperature fluctuations resulting in the generation of numerous high and low temperature blobs. These blobs are often referred to as entropy waves. It is now known that when entropy waves or entropy blobs are convected through a mean flow with significant axial velocity gradients, indirect combustion noise is generated (see figure 1). The present research is to investigate this phenomenon computationally.

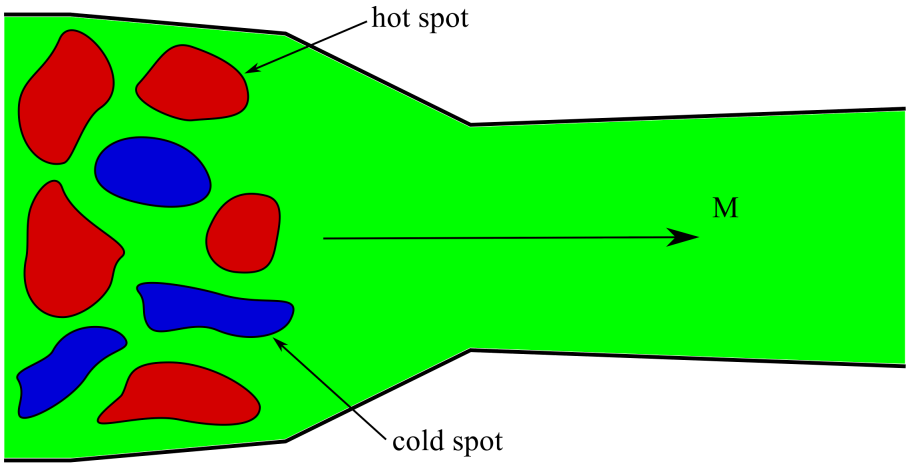

Figure 1. The passage of hot and cold spots of combustion from the afterburner through the convergent-divergent nozzle is the mechanism responsible for the generation of indirect combustion noise.

Two critical elements are required in any study of indirect combustion noise generation by numerical simulation in a military-styled nozzle. They are,
1. The creation of a random broadband entropy wave field as an input to the computation.
2. A mean flow inside the nozzle.

Once these two elements are established, a parametric study of indirect combustion noise can be carried out by passing the computed broadband entropy wave field through the mean flow inside the nozzle.

In this progress report, we will report the following.

A. The development of a stochastic entropy wave generation model to be used as input boundary condition in a numerical simulation. We will first report the development of a one-dimensional model as it is less complicated and hence easier to understand. Our report below includes the analytical model and validation tests. Then we report the extension to three-dimensions and validation test results.

   In developing our three dimensional stochastic entropy wave generation model, we prescribe the requirements that a user must be able to specify,
   a. The intensity of temperature fluctuations.
   b. The spectrum of fluctuations.
   c. The two-point cross correlation functions in two lateral perpendicular directions in the lateral plane perpendicular to the direction of the mean flow. These two-point temperature fluctuation cross-correlation functions are designed to allow a user to specify the lateral size of the entropy blobs.

B. The development of a high quality computational algorithm for computing the mean flow inside a military styled nozzle. This algorithm permits a user to prescribe all the mean flow variable at the inflow boundary. They include the pressure, temperature and density in addition to the inflow velocity and Mach number. One characteristic feature of a military-styled nozzle is that it has a fairly sharp throat. Because of the sharp throat shocks are, invariably, created inside the nozzle. Our algorithm, therefore, is designed with shock capturing capability.

II. Stochastic model boundary condition simulating incoming broadband entropy waves/blobs

A. One Dimensional Stochastic Entropy Wave Field Generation Model

We will use dimensionless variables with the following quantities as scales

λ_0 (the size of the dominant entropy blobs) as the length scale.

a_0 (speed of sound) as the velocity scale

λ_0 / a_0 as the time scale

ρ_0 as the density scale

$\rho_0 a_0^2$ as the pressure scale

For one dimensional compressible flow, the governing equations for entropy and acoustic waves in dimensionless forms are:

$$\frac{\partial T}{\partial t}+M\frac{\partial T}{\partial x}+\left(\gamma-1\right)\overline{T}\frac{\partial u}{\partial x}=0 \qquad (1)$$

$$\frac{\partial u}{\partial t}+M\frac{\partial u}{\partial x}+\frac{\overline{T}}{\gamma\overline{p}}\frac{\partial p}{\partial x}=0 \qquad (2)$$

$$\frac{\partial p}{\partial t}+M\frac{\partial p}{\partial x}+\gamma\overline{p}\frac{\partial u}{\partial x}=0 \qquad (3)$$

where an overbar indicates a mean flow quantity.

We will let the spectrum of the prescribed temperature fluctuations, $S\left(\omega\right)$, be as shown in figure 2.

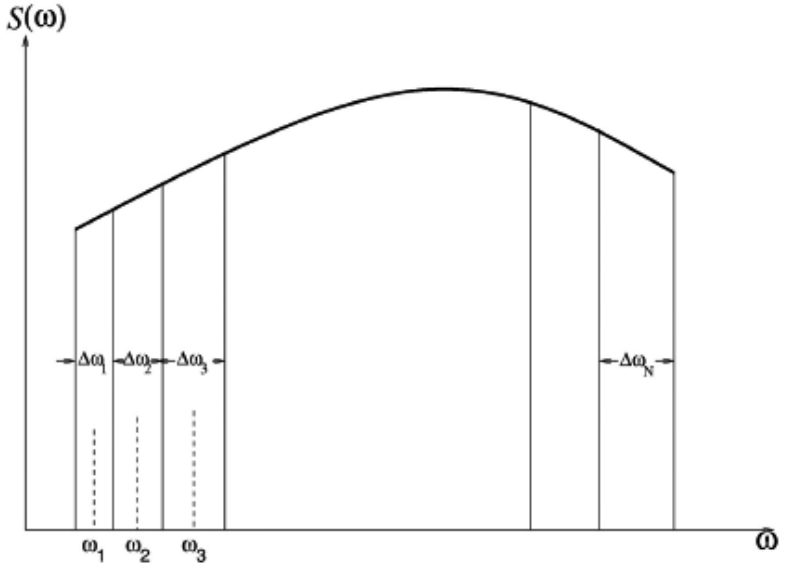

Figure 2. Discretization of the prescribed spectrum into multiple bands with width $\Delta\omega_j$.

We propose to discritize the given spectrum $S\left(\omega\right)$ into multiple narrow bands with center frequencies ω_j (*j=1 to N*) and bandwidth $\Delta\omega_j$ as shown in figure 2. The width of the narrow bands $\Delta\omega_j$ is random.

It is straightforward to show that the following stochastic temperature field satisfies governing equations (1), (2) and (3).

$$T=\sum_{j=1}^{N}A_j\cos\left[\omega_j\left(\frac{x}{M}-t\right)+\phi_j\right]$$
$$u=0 \qquad (4)$$
$$p=0$$

We may consider equation (4) as consists of multiple simple harmonic oscillators with frequencies at ω_j. To conserve energy, the amplitude A_j of each oscillator with frequency ω_j is given by,

$$\tfrac{1}{2}A_j^2 = 2S\left(\omega_j\right)\Delta\omega_j \tag{5}$$

To randomize the oscillators, in this model, the phase ϕ_j is to be a random number scaled to the range of $\left[0 \text{ to } 2\pi\right]$. So the random wave field given by equation (4) is created primarily by phase randomization.

To show that the model given by equation (4) would yield a stochastic field with a spectrum and intensity the same as the prescribed input i.e. $S\left(\omega\right)$ of figure 2, we can first compute the two-point space-time correlation function from the stochastic field generated by equation (4). By means of equation (4), after some lengthy algebra and the repeated use of the formula $\cos A\cos B = \tfrac{1}{2}\left[\cos(A-B)+\cos\left(A+B\right)\right]$ to reduce the product terms of cosines to a sum of cosines, it is straightforward to derive,

$$\overline{T\left(x',t'\right)T\left(x'',t'+\tau\right)} = \sum_{j=-N}^{N}\sum_{k=-N}^{N} 2\left[S\left(\omega_j\right)S\left(\omega_k\right)\Delta\omega_j\Delta\omega_k\right]^{\frac{1}{2}} \times \overline{\cos\left[\omega_j\left(\frac{x'}{M}-t'\right)+\phi_j\right]\cos\left[\omega_k\left(\frac{x''}{M}-t'-\tau\right)+\phi_k\right]} \tag{6}$$

where the overbar denotes a time average. Also,

$$\overline{\cos\left[\omega_j\left(\frac{x'}{M}-t'\right)+\phi_j\right]\cos\left[\omega_k\left(\frac{x''}{M}-t'-\tau\right)+\phi_k\right]} = \frac{1}{2}\cos\left[\omega_k\left(\frac{x''-x'}{M}-\tau\right)\right]\delta_{jk} \tag{7}$$

where δ_{jk} is the Kronecker delta. On substituting (7) into (6), the space-time cross-correlation function is found to be,

$$\overline{T\left(x',t'\right)T\left(x'',t'+\tau\right)} = \sum_{k=-N}^{N} S\left(\omega_k\right)\Delta\omega_k\cos\left[\omega_k\left(\frac{x''-x'}{M}-\tau\right)\right] \tag{8}$$

The autocorrelation function of the entropy field may be found by setting $x'' = x'$. This yields,

$$\overline{T^2\left(x',t'\right)} = \sum_{k=-N}^{N} S\left(\omega_k\right)\Delta\omega_k \to \int_{-\infty}^{\infty} S\left(\omega\right)d\omega; \text{ in the limit } \Delta\omega_k \to 0 \qquad (9)$$

Thus the spectrum of the stochastic entropy wave field generated by equation (4) will yield a spectrum equal to $S\left(\omega\right)$, the input spectrum.

Validation

To illustrate the effectiveness of our model, let's consider the following test case. Consider a one dimensional duct carrying a uniform mean flow of Mach number *M*. A stochastic entropy wave field enters the duct on the left end and exits on the right end. Let the size of the dominant hot spot be 1 in dimensionless unit. We would like to be able to resolve hot spots 0.2 times smaller that the dominant ones. To be able to do so, we will take,

$$\Delta x = 0.2/7 \approx 0.02$$

The factor $1/7$ above comes from the resolution of the DRP scheme that we intend to use in all our computations.

The entropy blobs are convected downstream by the mean flow. So, in one unit of dimensionless time, the flow moves a distance of M past a fixed point. The number of dominant hot spots passing this point per unit time is $M/1.0 = M$. Therefore, the dominant frequency of entropy blobs passing a point in the computational domain is M. Hence, the dominant angular frequency is $\omega_0 = 2\pi M$. We will use a Gaussian spectrum with the following parameters.

$$S\left(\omega\right) = e^{-\ln(2)\left[\frac{\omega-\omega_0}{b}\right]^2} + e^{-\ln(2)\left[\frac{\omega+\omega_0}{b}\right]^2} \qquad (10)$$

$$M = 0.3, \quad \omega_0 = 1.885, \quad b = \frac{\omega_0}{2.0}$$

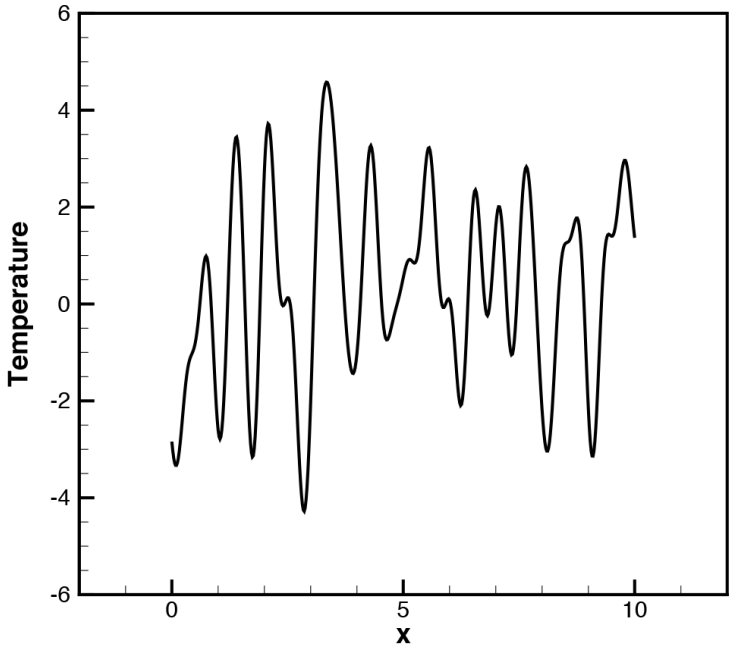

Figure 3. An instantaneous temperature distribution in the test duct taken from a numerical simulation.

To demonstrate the capability and accuracy of the model a computer code is developed to generate the stochastic broadband wave field according to equation (4). The computed space-time data of temperature is processed for comparison with model input functions. Figure 3 shows a computed instantaneous temperature distribution in the computation domain. The temperature field varies in space and time. There are approximately 10 blobs in the computational domain. This is expected, as the dominant entropy blob has a length of 1.0 in this test case. Figure 4 is a plot of the input spectrum (full line). Also shown is the spectrum computed from the numerical data of the simulation (dashed line) measured at $x = 5.0$. Figure 5 shows the input autocorrelation and the autocorrelation obtained by processing the numerical data. It is self-evident that there are good agreements between the input and numerical results in both figures 4 and 5. This provides support to the belief that the entropy wave generation model developed in this project is accurate and reliable.

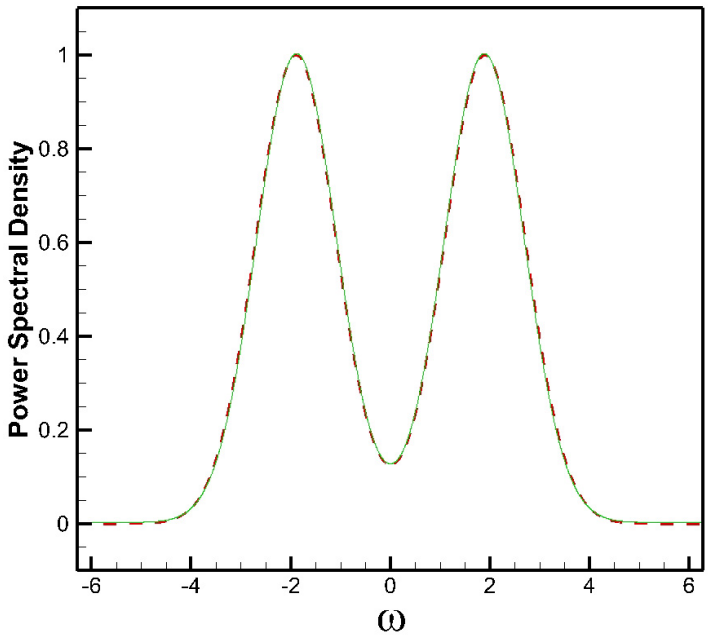

Figure 4. Comparison between input and computed power spectral density of the temperature fluctuations of the test example. Input (full line), processed from numerical data (dashed line)

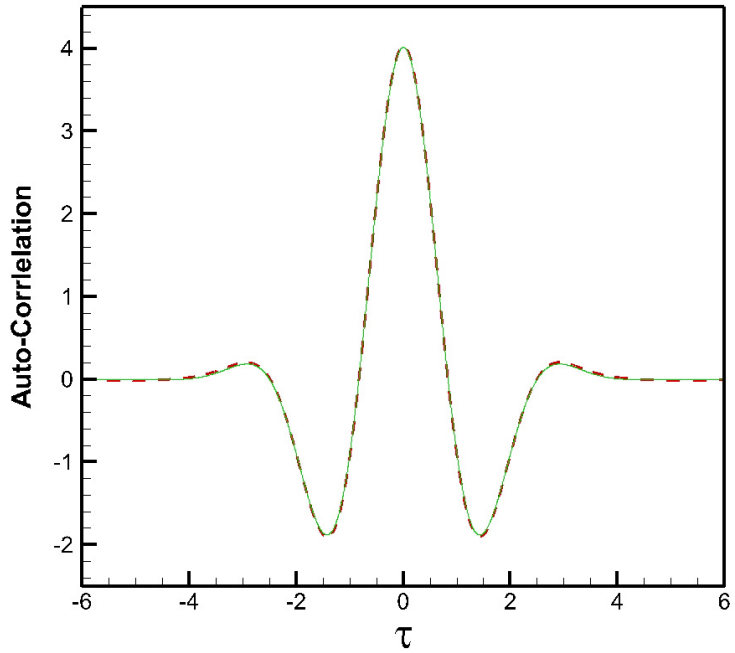

Figure 5. Comparison between input and computed autocorrelation function of the temperature fluctuations of the test example. Input (full line), processed from numerical data (dashed line)

Dr. Schuster of Honeywell provided us with his temperature fluctuation spectrum measured near the exit of the combustor of the Honeywell TECH977 turbofan engine. The spectrum is shown as a dashed line (reddish color) in figure 6. The smooth curve in this figure is the corresponding spectrum computed from data generated by our model

using Dr. Schuster's spectrum as input. There is excellent agreement over the entire frequency range up to 4000 Hz.

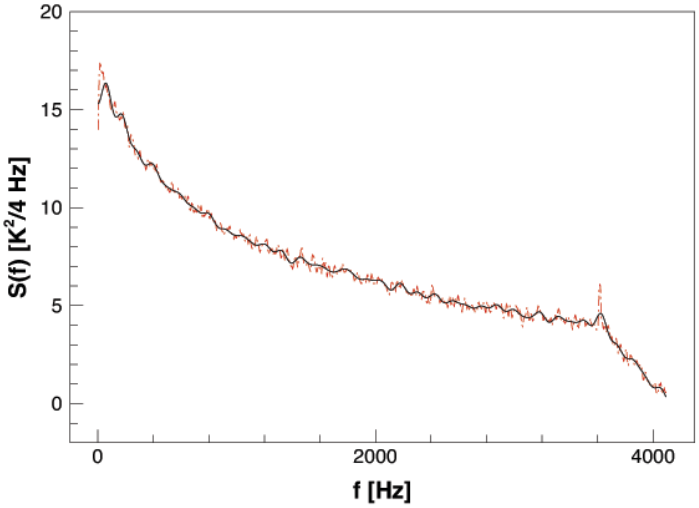

Figure 6. Temperature fluctuation spectrum measured by Schuster et al in their engine noise study using TECH 977.

B. Three Dimensional Stochastic Entropy Wave Field Generation Model

We have successfully generalized the one-dimensional model of equation (4) to three dimensions. In three dimensions, in addition to prescribing the intensity and spectrum of the random wave field, a user can prescribe the two-point cross correlation functions in two perpendicular directions in the lateral plane. The half-widths of these two-point cross correlation function serve as a measure of the lateral size of the random entropy blobs, Thus, if the x-axis is the direction of the mean flow, then one can prescribe the spectrum and the two-point cross correlation functions in the y and z directions.

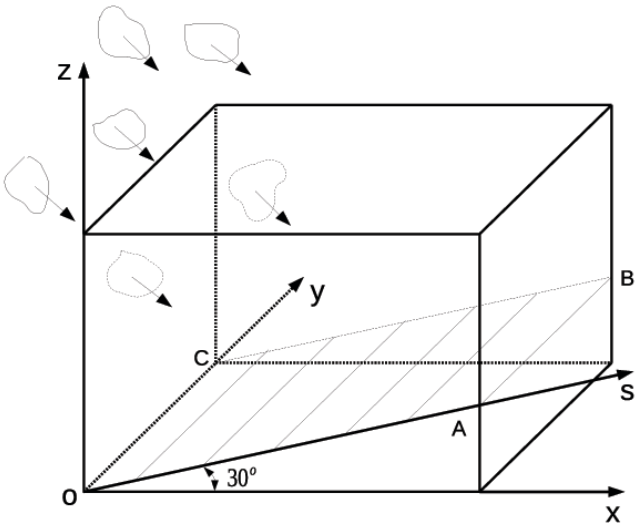

Figure 7. Inclined plane at 30^0 to the mean flow direction for observation of stochastic entropy wave field.

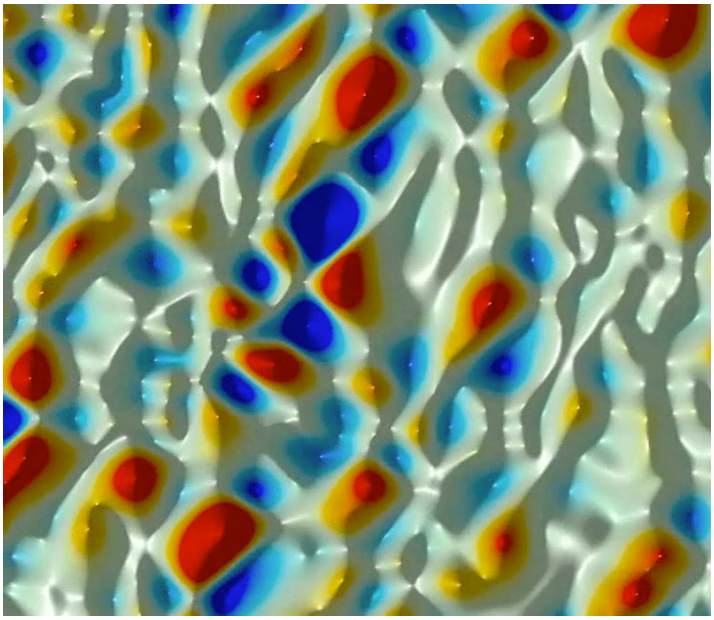

Figure 8. Stochastic entropy wave field generated by 3-D model with spectrum and lateral cross correlation function given by equations (11) to (13).

To illustrate the accuracy of the model, we consider the test case with the following spectrum and lateral cross correlation functions.

$$S(\omega)=\overline{T^2}\left(\frac{\ln 2}{\pi}\right)^{\frac{1}{2}}\frac{1}{2\sigma}\left[e^{-\ln 2\left(\frac{\omega-\omega_0}{\sigma}\right)^2}+e^{-\ln 2\left(\frac{\omega+\omega_0}{\sigma}\right)^2}\right] \tag{11}$$

$$\overline{T(x,y',z,t)T(x,y'',z,t)}=\overline{T^2}e^{-\ln 2\left(\frac{y'-y''}{b}\right)^2} \tag{12}$$

$$\overline{T(x,y,z',t)T(x,y,z'',t)}=\overline{T^2}e^{-\ln 2\left(\frac{z'-z''}{b}\right)^2} \tag{13}$$

The parameters are assigned the values below.

$$\overline{T^2}=1.0,\ \ b=0.75,\ M=0.3,\ \omega_0=2\pi M,\ \sigma=\omega_0/2$$

To see the entropy wave field in 3 dimensions, we consider the plane OABC in figure 7. The mean flow is in the x-y plane at 45^0 to the y-axis. Figure 8 shows the entropy wave field generated by the model as observed on the inclined plane of figure 7. In figure 8, red indicates high temperature and blue implies low temperature.

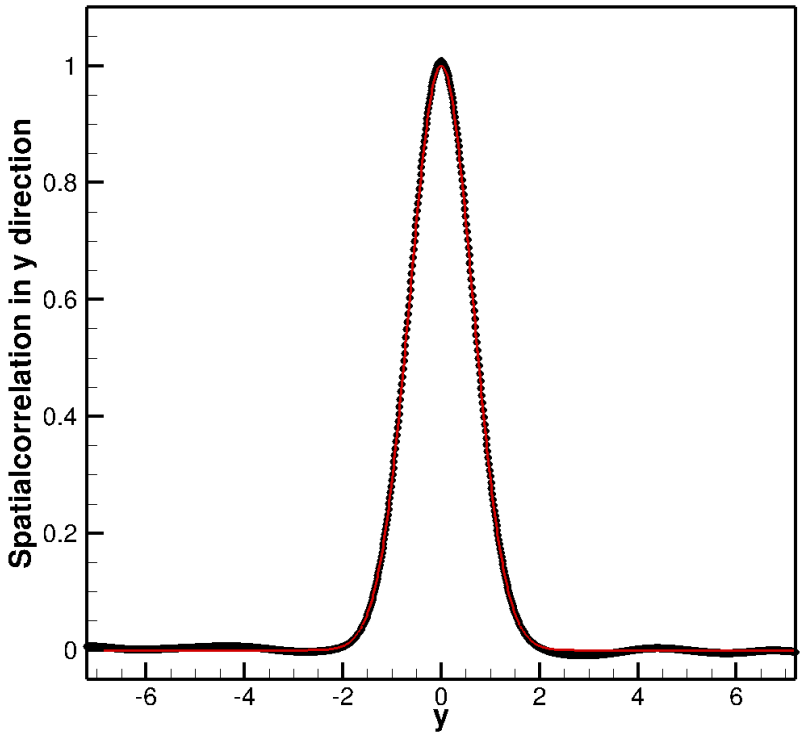

Figure 9. Comparison between input two-point cross correlation function and the computed cross correlation function. Here $y=(y'-y'')$.

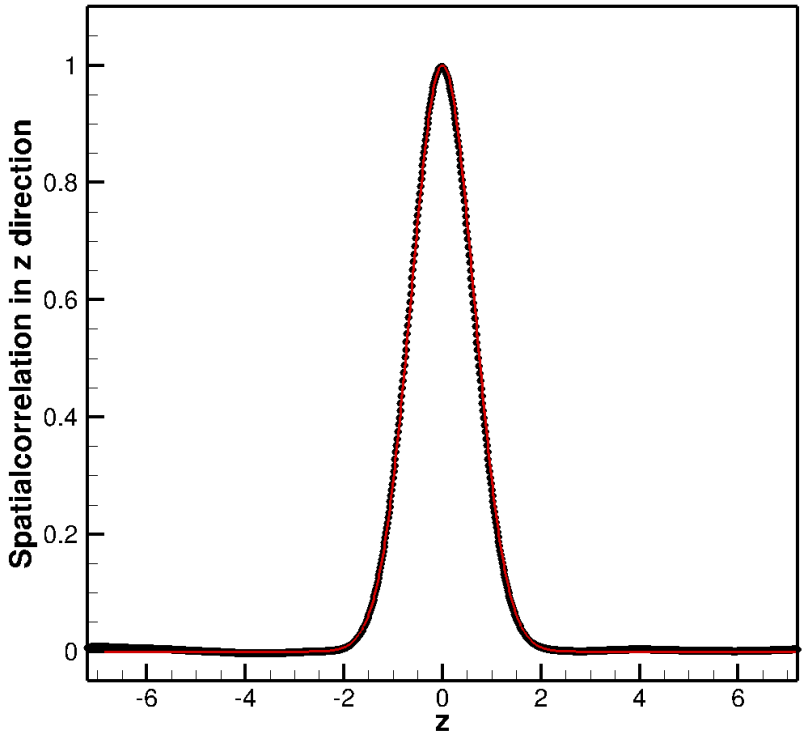

Figure 10. Comparison between input two-point cross correlation function and the computed cross correlation function. Here $z=(z'-z'')$.

Figure 9 shows a comparison of the two-point cross correlation function in the y-direction. The full line is the input function (equation 12). The black dots are the cross correlation function computed from the model generated stochastic temperature fluctuation field. There is excellent agreement. Figure 10 shows similar comparison in the z-direction. Again there is excellent agreement. Figure 11 shows a comparison between the input spectrum function and the spectrum function computed from model generated random field data. The agreement is again excellent. The excellent agreements provide a strong validation of the 3 dimensional model boundary condition developed in the present research effort.

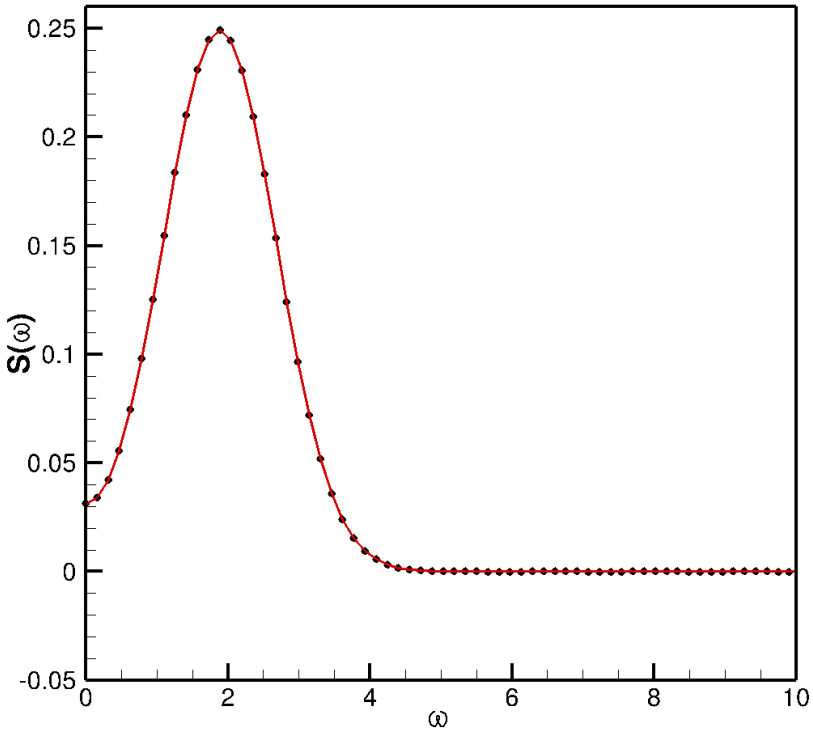

Figure 11. Comparison between input temperature fluctuation spectrum and the spectrum computed from stochastic temperature fluctuation field generated by the model boundary condition developed in the present research effort. Red line = input spectrum. Black dots = computed spectrum.

III. Computation of mean flow inside a military styled nozzle

Recently, Tam and Parrish (*Noise of High-Performance Aircraft at Afterburner* Journal of Sound and Vibration, **352**, 103-128, 2015) proposed that indirect combustion noise could be an important noise component of the F-22 aircraft at afterburner. F-22 aircraft have rectangular nozzle. To ensure a high chance of success, we will first investigate the generation of indirect combustion noise inside a rectangular nozzle. Figure 12 shows the upper half of the nozzle geometry and Mach number to be used in the present work. The exit Mach number 1.4 is based on a one dimensional compressible

flow calculation. For three dimensional flow, shocks will appear inside the nozzle so that the flow at the nozzle exit will not be uniform.

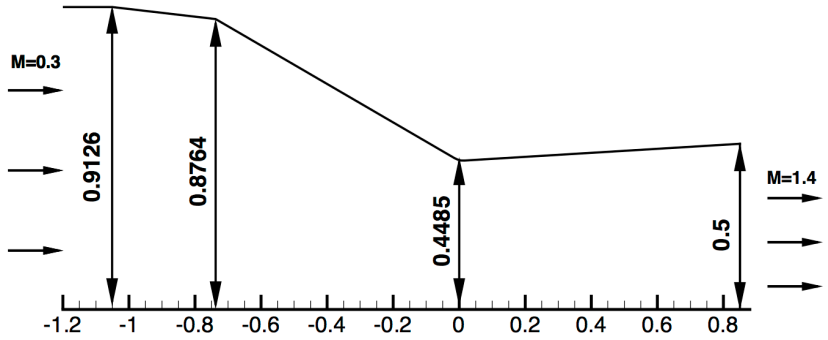

Figure 12. Geometry of the upper half of the rectangular military styled nozzle used in the present work.

We will use a body-fitted grid for numerical computation. This is done by applying the following mapping to the physical domain. Figure 13 illustrates the mapping of a curved domain into a rectangular domain. Let $y = y_a(x)$ and $y = y_b(x)$ be the bottom and top boundary of a curved domain as shown. The mapping function to be used is,

$$\xi = x \quad , \quad \eta = \frac{1}{y_a(x) - y_b(x)}\left[y(\eta_0 - \eta_e) + \eta_e y_a(x) - \eta_0 y_b(x) \right]$$

The end points η_0 and η_e are free parameters that one may choose to ensure that the mapped domain is rectangular.

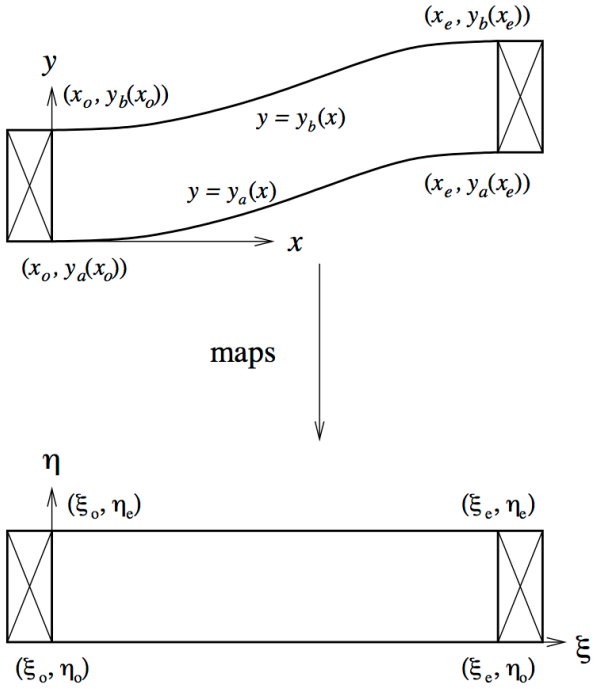

Figure 13. Mapping of a curved domain into a rectangular domain.

The mapping will transform the nozzle in the x-y plane into a rectangular domain in the $\xi-\eta$ plane. So the computational domain $\xi-\eta-z$ is a rectangular box. Because the two side plates of the nozzle are flat plates, the mean flow is two-dimensional. But with a 3 dimensional field of random entropy blobs as input, the indirect combustion noise generation process is three dimensional. Figure 14 shows the mean flow computational domain in the $\xi-\eta$ space. The height of the nozzle is h_0. $\xi=0$ is the location of the nozzle throat.

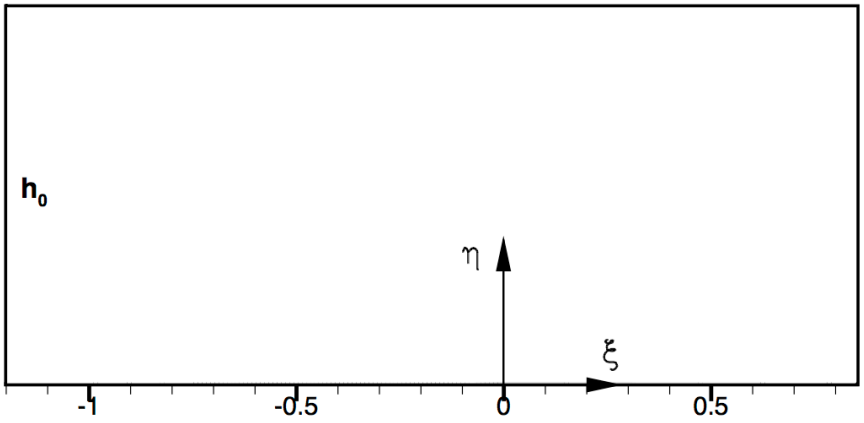

Figure 14. The computational domain in the $\xi-\eta$ plane.

The governing equations are the Euler equations and the energy equation. We use T, p, u and v as dependent variables. These equations are,

$$\frac{\partial T}{\partial t}+u\frac{\partial T}{\partial x}+v\frac{\partial T}{\partial y}+(\gamma-1)T\left[\frac{\partial u}{\partial x}+\frac{\partial v}{\partial y}\right]=0$$

$$\frac{\partial u}{\partial t}+u\frac{\partial u}{\partial x}+v\frac{\partial u}{\partial y}+\frac{T}{\gamma p}\frac{\partial p}{\partial x}=0$$

$$\frac{\partial v}{\partial t}+u\frac{\partial v}{\partial x}+v\frac{\partial v}{\partial y}+\frac{T}{\gamma p}\frac{\partial p}{\partial y}=0$$

$$\frac{\partial p}{\partial t}+u\frac{\partial p}{\partial x}+v\frac{\partial p}{\partial y}+\gamma p\left[\frac{\partial u}{\partial x}+\frac{\partial v}{\partial y}\right]=0$$

For computing the mean flow, the 7-point stencil Dispersion-Relation-Preserving (DRP) scheme is used. The DRP scheme is a highly accurate large stencil high-order scheme. To start the solution, the one dimensional solution is employed as the starting condition. The solution is time marched until a steady state solution is achieved.

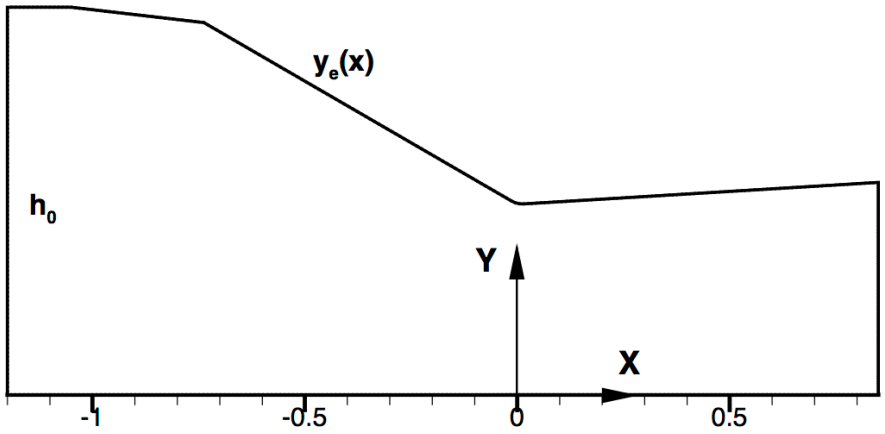

Figure 15. The physical domain of the upper half of a military styled nozzle.

Imposing correct boundary conditions is extremely important for acoustics problems. For the nozzle under consideration, the inflow enters the computational domain (see figure 15) from the left boundary and exits the domain through the right boundary. Since the nozzle is symmetric with respect to the center x-z plane, it is sufficient to compute the flow in the upper half of the nozzle. With this understanding, the following boundary conditions are enforced.

a. Left inflow boundary – a hard boundary condition with T, p, u and $v = 0$ is imposed. Because all the variables are prescribed, outgoing disturbances cannot leave from this boundary. They will all be reflected back into the computational domain and eventually exit from the outflow boundary on the right side.
b. At the top of the computational domain, the wall boundary condition is imposed.
c. At the bottom of the computational domain shown in figure 15, a symmetric boundary condition is enforced.
d. No boundary condition is needed at the right or exit boundary (see figure 15). This is because the flow at the nozzle exit is supersonic. No disturbance can propagate upstream against a supersonic flow.

In our computational algorithm, we include shock capturing capability. This is because the flow is supersonic downstream of the nozzle throat. We anticipate the sharp nozzle throat would lead to the formation of shocks inside the nozzle.

Numerical Results

Inside the nozzle, the flow is two-dimensional. In order to display the spatial distribution of the computed results, we plot the pressure and the mean flow velocity u along lines of constant η. Figure 16 shows these lines in the physical domain. Line 0 is the nozzle symmetric line. Line 7 corresponds to the top wall of the nozzle.

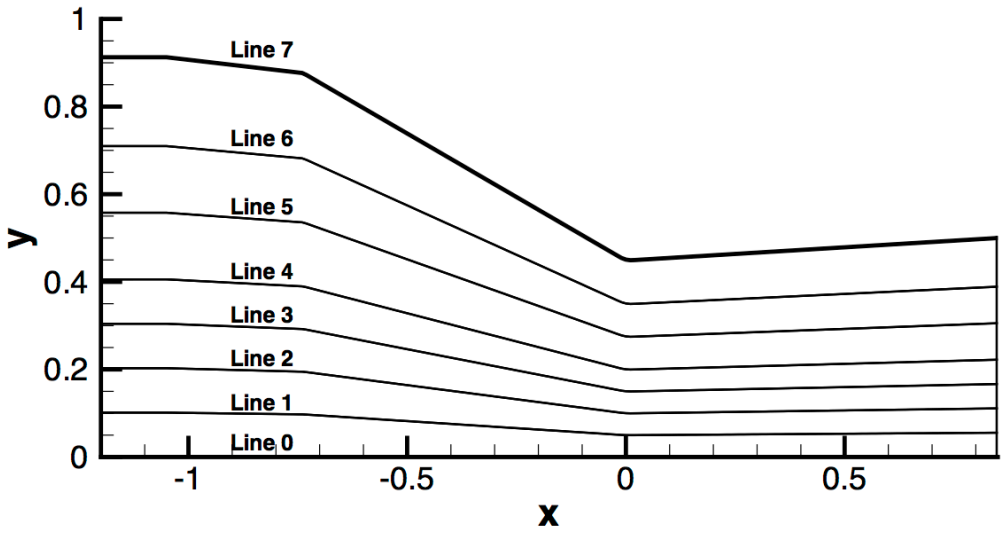

Figure 16. Lines of constant η in the physical domain along which computed results are shown.

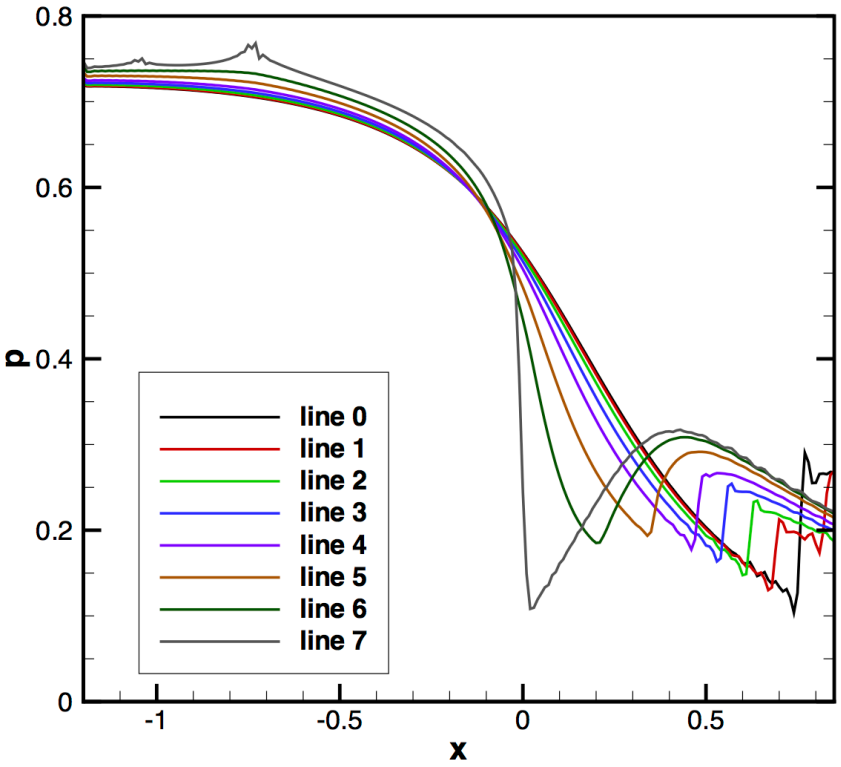

Figure 17. Pressure distributions as functions of x along the various lines shown in figure 16.

Figure 17 shows pressure distributions in the flow direction along the various line of figure 16. Line 7 is the pressure distribution along the upper wall of the nozzle. $x = 0$ is the location of the nozzle throat. This figure indicates that the static pressure drops in the flow direction. This pressure drop is the driving mechanism for a velocity increase in the flow direction inside the nozzle. Line 7, in particular, indicates that there is a sharp drop in pressure until the nozzle throat is reached. Beyond the throat, there is a pressure recovery. If we follow the pressure distribution along line 4, the pressure recovery is very abrupt. This means that a shock is formed. There is a sharp pressure rise in all the subsequent lines, namely, lines 3, 2, 1, and 0. The shock location propagates downstream and becomes closer and closer to the nozzle symmetric plane. Figure 18 shows the location of the shock inside the nozzle. The shocks from the top and bottom half of the nozzle intersect near the nozzle exit. They pass through each other before exiting outside the nozzle.

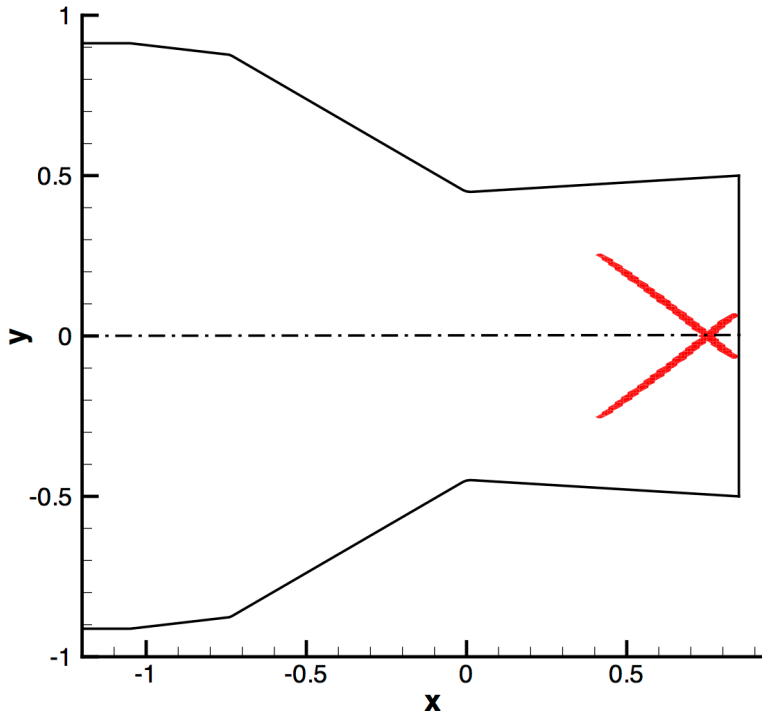

Figure 18. Location of shocks (red) inside the military styled nozzle.

Figure 19 shows the axial distribution of mean flow velocity u along line 7 of figure 16. There is a sharp drop in u for line 0 to line 4. They are the corresponding velocity jumps across the shock.

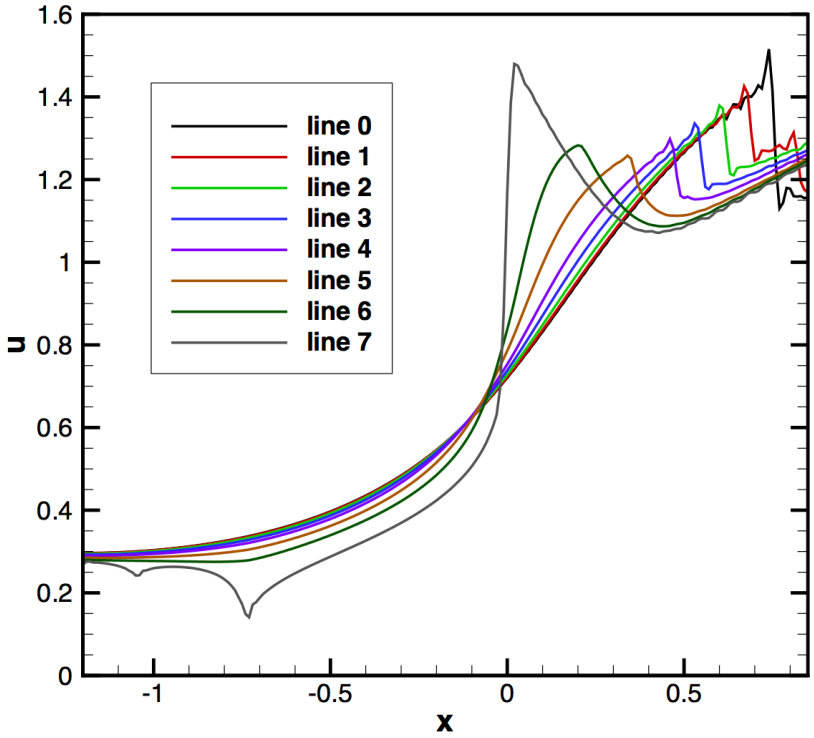

Figure 19. Axial distribution of mean flow velocity u along various lines of figure 16.

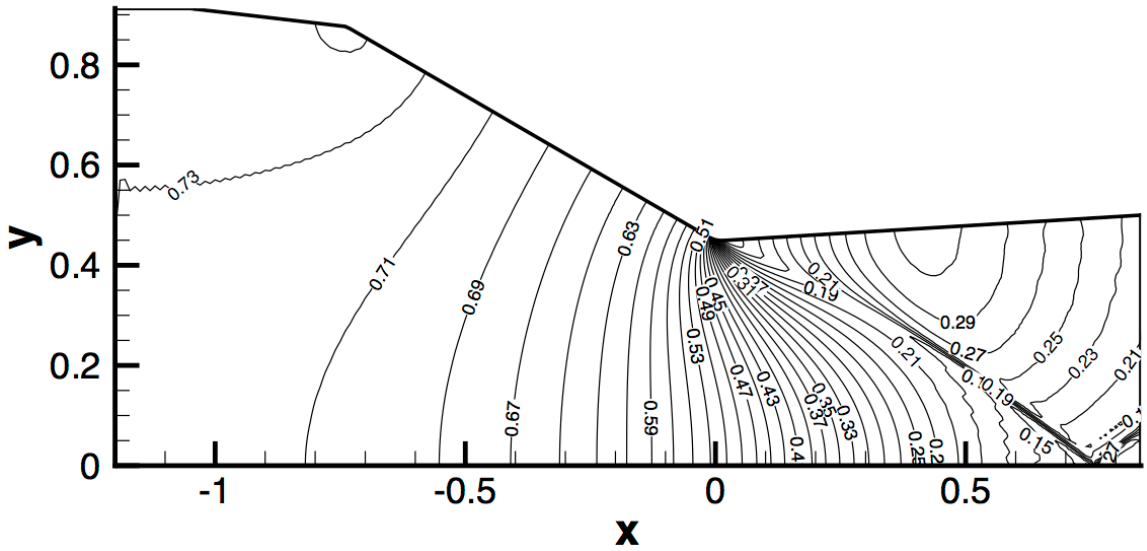

Figure 20. Distribution of pressure contours inside the military styled nozzle.

Figure 20 are pressure contours inside the nozzle. Near the nozzle exit the pressure contours merge into a sharp discontinuity. This is just another indication of the presence of a shock and a transmitted shock near the exit of the nozzle.

It is know that small disturbances such as vorticity waves will generate sound when passing through a shock wave. We expect the same is true when entropy blobs are convected through an oblique shock. This mechanism of sound generation has not been studied before. Our present investigation may help to shed light on the effectiveness of this shock-entropy wave interaction mechanism of noise generation.

IV. Future research

Currently we are in the process of developing a parallel multi-core computer code for computing indirect combustion noise generation caused by the passage of a stochastic entropy wave field through the mean flow inside a military styled nozzle. We expect the code development to be completed soon. We will then perform validation tests. Once this step is completed, we will perform a parametric study to determine the level, the spectrum and other features of the indirect combustion noise field that is generated inside the nozzle of a military aircraft.

REPORT DOCUMENTATION PAGE

Form Approved
OMB No. 0704-0188

1. REPORT DATE *(DD-MM-YYYY)*	2. REPORT TYPE	3. DATES COVERED *(From - To)*
22/09/2016	Quarterly Progress Report	06/15/2016 to 09/14/2016

4. TITLE AND SUBTITLE

Noise of High-Performance Aircraft at Afterburner

5a. CONTRACT NUMBER

5b. GRANT NUMBER

N00014-15-1-2008

5c. PROGRAM ELEMENT NUMBER

6. AUTHOR(S)

5d. PROJECT NUMBER

5e. TASK NUMBER

5f. WORK UNIT NUMBER

7. PERFORMING ORGANIZATION NAME(S) AND ADDRESS(ES)

Sponsored Research Administration, Florida State University, 874 Traditions Way
Tallahassee, FL 32306-4166

8. PERFORMING ORGANIZATION REPORT NUMBER

035259

9. SPONSORING/MONITORING AGENCY NAME(S) AND ADDRESS(ES)

Office of Naval Research AEROSPACE SCIENCE RESEARCH DIV 875 N. Randolph Street
Arlington, VA 22203-1995

10. SPONSOR/MONITOR'S ACRONYM(S)

ONR

11. SPONSOR/MONITOR'S REPORT NUMBER(S)

12. DISTRIBUTION/AVAILABILITY STATEMENT

DISTRIBUTION STATEMENT A: Approved for public release: distribution unlimited

13. SUPPLEMENTARY NOTES

14. ABSTRACT

Numerical simulation of the generation of indirect combustion noise in a military styled nozzle at afterburner

15. SUBJECT TERMS

16. SECURITY CLASSIFICATION OF:			17. LIMITATION OF ABSTRACT	18. NUMBER OF PAGES	19a. NAME OF RESPONSIBLE PERSON
a. REPORT	b. ABSTRACT	c. THIS PAGE			Christopher Tam
U	U	U	UU	20	19b. TELEPHONE NUMBER *(Include area code)* 850-644-2455